Earth and Planetary Science Letters 431 (2015) 110–118

Contents lists available at ScienceDirect

Earth and Planetary Science Letters

www.elsevier.com/locate/epsl

s-Process Os isotope enrichment in ureilites by planetary processing

S. Goderis [a,b,c,*], A.D. Brandon [c], B. Mayer [d], M. Humayun [d]

[a] Earth System Science, Vrije Universiteit Brussel, Brussels, Belgium
[b] Department of Analytical Chemistry, Ghent University, Ghent, Belgium
[c] Department of Earth and Atmospheric Sciences, University of Houston, Houston, TX, USA
[d] National High Magnetic Field Laboratory and Department of Earth, Ocean & Atmospheric Science, Florida State University, Tallahassee, FL, USA

ARTICLE INFO

Article history:
Received 17 April 2015
Received in revised form 1 September 2015
Accepted 12 September 2015
Available online xxxx
Editor: B. Marty

Keywords:
Os isotopes
ureilites
planetary processes
presolar grains
nucleosynthetic anomalies

ABSTRACT

Ubiquitous nucleosynthetic isotope anomalies relative to the terrestrial isotopic composition in Mo, Ru, and other elements are known from both bulk chondrites and differentiated meteorites, but Os isotope ratios reported from such meteorites have been found to be indistinguishable from the terrestrial value. The carriers of s- and r-process Os must thus have been homogeneously distributed in the solar nebula. As large Os isotope anomalies are known from acid leachates and residues of primitive chondrites, the constant relative proportions of presolar s- and r-process carriers in such chondrites must have been maintained during nebular processes. It has long been assumed that partial melting of primitive chondrites would homogenize the isotopic heterogeneity carried by presolar grains. Here, ureilites, carbon-rich ultramafic achondrites dominantly composed of olivine and low-Ca pyroxene, are shown to be the first differentiated bulk Solar System materials for which nucleosynthetic Os isotope anomalies have been identified. These anomalies consist of enrichment in s-process Os heterogeneously distributed in different ureilites. Given the observed homogeneity of Os isotopes in all types of primitive chondrites, this Os isotope variability among ureilites must have been caused by selective removal of s-process-poor Os host phases, probably metal, during rapid localized melting on the ureilite parent body. While Mo and Ru isotope anomalies for all meteorites measured so far exhibit s-process deficits relative to the Earth, the opposite holds for the Os isotope anomalies in ureilites reported here. This might indicate that the Earth preferentially accreted olivine-rich restites and inherited a s-process excess relative to smaller meteorite bodies, consistent with Earth's high Mg/Si ratio and enrichment of s-process nuclides in Mo, Ru, and Nd isotopes. Our new Os isotope results imply that caution must be used when applying nucleosynthetic isotope anomalies as provenance indicators between different classes of meteorites.

© 2015 Elsevier B.V. All rights reserved.

1. Introduction

Isotopic anomalies are defined as deviations from terrestrial or bulk solar isotopic abundances that have resulted from processes other than radioactive decay or mass-dependent fractionation. Presolar grains, widespread in unequilibrated chondrites, are enriched in material derived from distinct nucleosynthetic environments (Zinner, 1998). Small but resolvable isotopic anomalies in bulk meteorites, often most prominent in primitive carbonaceous chondrites, are present for various elements including Ti, Cr, Ni, Zr, Mo, Ru, Ba, Nd, and Sm (e.g., Akram et al., 2015; Burkhardt et al., 2011, 2012; Carlson et al., 2007; Chen et al., 2010; Dauphas et al., 2002; Qin et al., 2010; Regelous et al., 2008; Trinquier et al., 2009; Yin et al., 2002). Uniform isotopic compositions in bulk chondrites are reported for other elements, most prominently Os and Hf (Brandon et al., 2005; Sprung et al., 2010; van Acken et al., 2011; Walker, 2012; Wittig et al., 2013; Yokoyama et al., 2007). The presence of isotope anomalies in bulk planetary materials, such as chondrites and achondrites, is explained by a variety of mechanisms that resulted in isotope heterogeneity at the planetesimal scale. These include, for example, inheritance from a heterogeneous molecular cloud core, formation of localized heterogeneities due to differential physical sorting of dust grains (e.g., metals, silicates and sulfides), late supernova injection, or selective destruction of thermally labile presolar carrier phases in the nebula (e.g., Andreasen and Sharma, 2007; Burkhardt et al., 2011; Carlson et al., 2007; Chen et al., 2010; Dauphas et al., 2002; Qin et al., 2008; Trinquier et al., 2009). Alternatively, secondary processes, such as aqueous alteration have been suggested to selec-

* Corresponding author at: Earth System Science, Analytical, Environmental, and Geo-Chemistry (AMGC), Vrije Universiteit Brussel, Pleinlaan 2, B-1050 Brussels, Belgium. Tel.: +32 26291480.
E-mail address: Steven.Goderis@vub.ac.be (S. Goderis).

http://dx.doi.org/10.1016/j.epsl.2015.09.021
0012-821X/© 2015 Elsevier B.V. All rights reserved.

tively redistribute isotopically distinct components within a planetesimal (Yokoyama et al., 2011).

Osmium is an important element in this discussion, as it is one of the most refractory metals. Chemical residues and leachates of various chondrites of low metamorphic grade show complementary Os isotope anomalies, attributed to the presence of varying proportions of presolar grains carrying s-, r-, and possibly p-process Os (Brandon et al., 2005; Reisberg et al., 2009; van Acken et al., 2011; Yokoyama et al., 2007, 2010, 2011). Analyses of bulk chondrites using total digestion methods, thermally metamorphosed chondrites, and iron meteorites, however, have shown no evidence for resolvable Os isotopic heterogeneity within the current level of analytical resolution (Brandon et al., 2005; van Acken et al., 2011; Walker, 2012; Wittig et al., 2013; Yokoyama et al., 2007, 2010, 2011). This indicates that, although carriers with distinct Os isotopic compositions were present in the protosolar nebula, their relative proportions were fixed in all primitive chondrites, consistent with a well-mixed solar nebula (Brandon et al., 2005; Sprung et al., 2010; Yokoyama et al., 2007; Walker, 2012). Since low-grade metamorphism is sufficient to destroy presolar grains (Huss and Lewis, 1995), it has been assumed that partial melting should eliminate any small-scale Os isotope anomalies in the sources of differentiated bodies. The existing high-precision Os isotope data indicate that iron meteorites have the same Os isotopic composition as chondrites, consistent with homogenization of isotopically diverse components during melting and core formation (Walker, 2012; Wittig et al., 2013).

Ureilites are coarse-grained ultramafic achondrites, consisting primarily of olivine and pigeonite, with minor augite and orthopyroxene, abundant carbon (<7 wt%, graphite and diamond) and accessory metal and sulphides (e.g., Barrat et al., 2015; Goodrich et al., 2004; Warren et al., 2006). Ureilites are widely considered to represent mantle restites, formed after the extraction of silicate partial melts and S-rich metallic melts (e.g., Goodrich et al., 2004; Warren and Kallemeyn, 1992). Highly siderophile elements confirm that metallic liquids were extracted from ureilites with most ureilite metal having enrichments in compatible siderophile elements (Goodrich et al., 2013; Horstmann et al., 2014; Rankenburg et al., 2008). The heavy Fe isotopic composition of ureilites compared to chondrites corroborates an efficient segregation of S-rich metallic melts in the ureilite body, likely before the onset of silicate melting, and is interpreted to represent the early stages of asteroidal core formation (Barrat et al., 2015). Despite evidence of an igneous origin, ureilites also appear to have preserved primordial signatures in light stable isotopes. The ureilites do not follow a unique mass-dependent isotopic fractionation trend in oxygen isotope space (Clayton and Mayeda, 1996). Instead, ureilites trend along the carbonaceous chondrite anhydrous minerals (CCAM) line (Supplementary Fig. 1). Ureilites exhibit ^{33}S isotope enrichment (Farquhar et al., 2000), and large differences in δ^{15}N between diamond, graphite, and silicate phases (Rai et al., 2003a). These isotopic heterogeneities likely reflect primordial nebular heterogeneity of the accreting precursor materials and thus argue against magmatic equilibration of the ureilite parent body (UPB). Isotopic data for Cr, Ti, and Ni for ureilites (e.g., Regelous et al., 2008; Trinquier et al., 2009) add to the enigma of ureilites, as the reported ε^{50}Ti, ε^{54}Cr, and ε^{62}Ni (with the ε-notation representing isotopic deviations from a reference value in parts per 10,000) show the lowest (negative) values of all meteorites, grouping far from the carbonaceous chondrites that are themselves separated by a wide margin from all other planetary materials (Warren, 2011).

Following the earlier work of Rankenburg et al. (2007, 2008) on highly siderophile element abundances and ^{187}Os/^{188}Os isotope ratios, we obtained the first high-precision Os isotope data for a suite of mostly monomict ureilites using negative thermal ionization mass spectrometry (N-TIMS). This is the first high-precision isotope data obtained for ureilites for elements beyond the Fe-peak. Isotope dilution concentration data for highly siderophile elements (HSE: Ru, Pd, Re, Os, Ir, and Pt) are also reported on the same samples, to correct for radiogenic contributions from ^{187}Re and ^{190}Pt to ^{187}Os and ^{186}Os, respectively. Serendipitously, the high-precision Os isotope data revealed nucleosynthetic isotope anomalies. These data are used to place constraints on the genesis and early evolution of UPB reservoirs. Studying the Os isotopic signatures of ureilites provides a way to test possible large-scale heterogeneity linked to the inhomogeneous distribution of presolar material in the nascent solar nebula, and to evaluate the effects of planetary processes, such as partial melting, on the distribution of the carriers of nucleosynthetic isotope anomalies during planetary differentiation.

2. Materials and methods

Twelve monomict ureilite breccia samples were obtained from the Smithsonian Institution's National Museum of Natural History (Goalpara, Kenna), the NASA Meteorite Work Group (ALHA 81101, EET 87517, GRA 95205, GRA 98032, META 78008), and the Japanese National Institute of Polar Research (A 881931, Y 790981, Y 791538, Y 981750, Y 981810). Libyan Desert find DaG 319, the only polymict ureilite studied in this work, was purchased from a commercial meteorite dealer. Prior to dissolution, all surfaces on all pieces of meteorites were polished using carborundum, after which the meteorites were manually ground with a ceramic alumina mortar and pestle. In the methodology applied, high-precision determination of Os isotope ratios on unspiked digestions (Supplementary Table 1; Table 1) is combined with determination of elemental abundance ratios of Re, Os, Ir, Ru, Pt, and Pd, on small aliquots taken from the unspiked digestions to ensure the representativeness of these ratios for each sample digestion. In this way, ^{186}Os and ^{187}Os contributions generated by the long-lived radioactive ^{187}Re–^{187}Os and ^{190}Pt–^{186}Os decay systems with half-lives of 41.5 Ga and 488 Ga, respectively (Begemann et al., 2001; Smoliar et al., 1996), can be taken into account. Elemental ratios of interest are also checked by comparison to previously published data on the same meteorites (Table 2 and Fig. 1; Rankenburg et al., 2007, 2008). In order to obtain the amount of Os required for the high-precision Os isotope ratio measurements (~100 ng), each sample was digested in one to six carius tubes (CTs), depending on the Os concentration in the sample (ALHA 81101 and A 881931 with <80 ppb Os were digested in 6 and 3 CTs, respectively). For the initial unspiked digestions, ~0.5 g of sample powder was digested in acid leached borosilicate glass CTs for 48 h at 230 °C with 3 ml conc. HCl and 6 ml conc. HNO_3. After that, the tubes were frozen and opened, and 0.45 ml of the acid sample solution from one of the CTs representing a single sample digestion transferred into a quartz CT for precise determination of elemental abundances of the ureilites. After an aliquot of digested sample solution was transferred, the quartz CT was chilled and an appropriate amount of mixed ^{99}Ru–^{110}Pd–^{185}Re–^{190}Os–^{191}Ir–^{198}Pt spike (#000601) was added, followed by 1 ml of conc. HCl and 2 ml of conc. HNO_3. Sample-spike equilibration was achieved in an oven at 230 °C for 24 h after sealing of the CTs. Where samples were split across several CTs, the Pt/Os ratios obtained for one of these CTs were compared either to literature data (ALHA 81101) or duplicate analysis of the same sample powder (A 881931) and found indistinguishable within uncertainty (Table 2). Regardless, ^{190}Pt/^{188}Os radiogenic corrections were found to be marginal compared to the observed nucleosynthetic effects (Table 1, Supplementary Table 1).

Unspiked aliquot Os from the batch of CTs containing a single sample digestion was extracted using CCl_4/HBr solvent extraction (Cohen and Waters, 1996), subsequently purified using

Table 1
High-precision Os isotopic composition of ureilites, expressed in ε- and μ-units compared to average equilibrated ordinary chondrite values (Brandon et al., 2005). The complete data set detailing UMD Os standard values and equilibrated ordinary chondrite data used for normalization is given in Supplementary Table 1. $\mu^{186}Os_i$ are corrected to 4.562 Ga. The $2\sigma_{mean}$ uncertainties on $\mu^{186}Os_i$ include propagation of the Pt/Os ratio uncertainties.

	ε^{184}Os	$2\sigma_{mean}$	μ^{186}Os	$2\sigma_{mean}$	$\mu^{186}Os_i$	$2\sigma_{mean}$	μ^{188}Os	$2\sigma_{mean}$	μ^{190}Os	$2\sigma_{mean}$
ALHA 81101	15.0	6.2	319.9	10.6	336.0	12.5	60.4	3.6	34.1	2.2
Y 791538	17.5	3.6	138.9	6.9	165.2	8.6	36.9	2.5	14.5	1.4
A 881931	−5.7	6.5	76.6	11.4	107.7	13.0	16.4	4.0	6.8	2.4
DaG 319	12.1	8.8	62.8	14.3	79.6	16.2	19.3	4.7	6.7	3.1
EET 87517	1.6	8.0	17.8	12.5	38.0	14.3	9.6	4.3	1.1	2.5
Kenna	16.4	3.7	−23.9	7.5	7.5	9.0	8.3	2.9	−5.9	1.5
Y 981750	7.7	5.4	5.6	9.0	13.6	11.0	7.9	4.2	3.8	2.1
Y 981810	33.8	4.2	−69.9	6.8	−7.0	7.7	0.2	2.5	−7.7	1.6
META 78008	12.7	4.7	−54.7	8.0	10.3	8.9	8.8	2.9	−4.2	1.7
Y 790981	14.8	4.0	−21.9	6.6	−2.0	8.4	0.4	2.5	−8.0	1.5
GRA 95205	−6.4	6.1	−58.7	10.4	−2.2	11.5	8.2	3.5	1.9	2.1
Goalpara	24.1	6.1	−39.2	9.8	1.1	11.2	1.9	3.7	−4.2	2.1
GRA 98032	18.5	2.8	−37.3	5.0	−1.9	6.4	4.6	1.9	−8.2	1.1

Table 2
Highly siderophile element concentrations of ureilites analyzed for high-precision Os isotopes.

	Mineral ass.	Shock level		Re (ppb)	Re_c	Os (ppb)	Ir (ppb)	Ru (ppb)	Pt (ppb)	Pd (ppb)	Re/Os	Pt/Os	^{190}Pt/^{188}Os
ALHA 81101	ol-pig	High/very high		1.9	2.4	43.5	32.7	49.7	73.9	51.5	0.043	1.70	0.001619
			lit.	1.9	1.9	33.6	30.8	46.9	55.6	33.0	0.057	1.65	0.001576
Y 791538	ol-opx	Medium		6.7	15.0	184	152	209	277	59.9	0.037	1.51	0.001437
A 881931	ol-pig			4.6	5.9	78.8	65.1	101	112	74.8	0.058	1.42	0.001354
			dupl.	4.4		68.2	54.1	76.3	92.6	60.6	0.064	1.36	0.001293
DaG 319	polymict	Low		10.4	22.9	283	208	313	477	92.0	0.037	1.69	0.001605
			lit.	10.3	18.3	226	207	317	420	77.4	0.046	1.86	0.001770
			lit.	10.8	19.1	234	226	342	434	96.8	0.046	1.85	0.001766
EET 87517	ol-opx	Low		138	26.8	347	254	385	563	128	0.397	1.62	0.001546
			lit.	18.4	24.9	322	291	446	587	128	0.057	1.82	0.001736
Kenna	ol-pig	Medium		31.2	40.9	497	394	498	703	67.3	0.063	1.41	0.001347
			lit.	33.6	41.6	504	427	614	710	60.2	0.067	1.41	0.001342
			lit.	31.8	39.7	476	434	594	739	–	0.067	1.55	0.001479
Y 981750	ol-minor px			35.2	26.6	331	354	463	613	154	0.106	1.85	0.001763
Y 981810	ol-minor px			56.1	84.9	1000	679	720	827	89.2	0.056	0.83	0.000788
META 78008	+aug	Medium		51.0	77.3	904	470	710	712	101	0.056	0.79	0.000750
			lit.	65.7	98.1	1071	751	1122	1040	118	0.061	0.97	0.000925
Y 790981	ol-pig			21.8	21.2	265	213	309	432	143	0.082	1.63	0.001551
GRA 95205	ol-pig	Medium/high		62.0	57.7	670	419	492	633	60.0	0.093	0.95	0.000901
			lit.	74.1	74.2	869	661	758	831	84.3	0.085	0.96	0.000911
			lit.	58.0	68.4	791	588	590	654	77.5	0.073	0.83	0.000787
Goalpara	ol-pig	High		8.3	9.5	118	83.2	118	148	39.9	0.070	1.25	0.001189
			lit.	8.8	8.7	109	88.9	126	157	41.1	0.081	1.44	0.001372
			lit.	8.9	8.5	107	87.9	122	151	44.6	0.083	1.41	0.001344
GRA 98032	ol-pig	High		23.3	24.3	293	227	291	393	45.9	0.080	1.34	0.001278
			lit.	41.5	26.3	314	236	321	362	47.7	0.132	1.15	0.001098
			lit.	29.3	25.7	308	230	325	380	47.8	0.095	1.23	0.001175
			lit.	21.4	26.5	319	251	334	406	45.2	0.067	1.27	0.001212
CI chondrite			lit.	37.2		449	424	631	864	563	0.083	1.92	0.001833

Re_c, Re concentrations calculated from Os concentrations and Os isotope ratios (Table 1) assuming an age of 4562 Ma; dupl., duplicate acquired in a different session; lit., literature data from Rankenburg et al. (2008) for ureilites; CI chondrites, average Orgueil and Ivuna from Walker et al. (2002), Horan et al. (2003), and Fischer-Gödde et al. (2010). Mineral ass., mineral assemblage; ol, olivine; pig, pigeonite; opx, orthopyroxene; +aug, augite-bearing. Prefixes of Antarctic samples: A, Asuka; ALH, Allan Hills; EET, Elephant Moraine; GRA, Graves Nunataks; MET, Meteorite Hills; Y, Yamato.

H_2SO_4/H_2CrO_4 microdistillation (Birck et al., 1997), and combined into a single fraction. For N-TIMS measurement, Os was loaded on Pt filaments (H. Cross Company™) in HBr and run in negative ion mode as OsO_3^- on a ThermoFisher Triton Plus at the University of Houston. Static high-precision measurements consisted of 420 to 2100 cycles with 16 s of integration time and virtual amplifier rotation every 20 cycles. Isobaric interferences attributable to W- or Pt-oxides were either not observed or were found to be negligible (Brandon et al., 2005). Repeated measurements of ∼100 ng loads of the UMD Johnson Matthey Os standard were conducted to monitor reproducibility of isotope ratio measurements and cup drift (Supplementary Table 1). Over the course of the measurement campaign (July 2013 to March 2014), this standard yielded $^{184}Os/^{188}Os$ of 0.0013052 ± 53, $^{186}Os/^{188}Os$ of 0.1198458 ± 23, $^{187}Os/^{188}Os$ of 0.1137841 ± 24, $^{189}Os/^{188}Os$ of 1.219673 ± 12, and $^{190}Os/^{188}Os$ of 1.983788 ± 20 (2σ, $n = 13$) using $^{192}Os/^{188}Os = 3.083$ as reference for fractionation correction with an exponential law (e.g., Brandon et al., 2005; van Acken et al., 2011). The uncertainty on the average initial $^{186}Os/^{188}Os$ ratio calculated for the ureilites showing no nucleosynthetic anomalies, 0.1198265 ± 8 as shown in Fig. 2, is determined by dividing the external precision of the isotopic analysis (±19 ppm) by the square root of the number of non-anomalous ureilites (8). Because ^{189}Os and ^{192}Os contain the smallest contribution from the nucleosynthetic s-process (4.8% and 0.4%, respectively; Arlandini et al., 1999), normalization to $^{192}Os/^{189}Os = 2.527686$ is required to study nucleosynthetic isotope variation. Using this normalization scheme, the standard yielded values for $^{184}Os/^{189}Os$ of 0.0010702 ± 46, $^{186}Os/^{188}Os$ of 0.0982619 ± 37, $^{188}Os/^{189}Os$ of 0.819897 ± 11, and $^{190}Os/^{189}Os$ of 1.626484 ± 26 (2σ). Standards and samples were

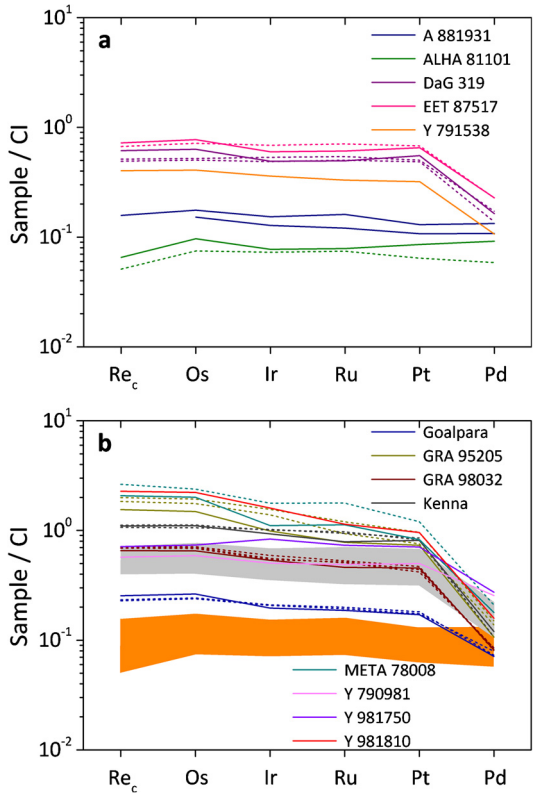

Fig. 1. Highly siderophile element abundances in ureilites normalized to mean CI chondrites (Table 1) arranged according to 50% condensation temperature. Rhenium abundances are calculated from $^{187}Os/^{188}Os$ isotope ratios and measured Os abundances to eliminate scatter introduced from increased Re mobility during terrestrial weathering (Rankenburg et al., 2007). Ureilites showing nucleosynthetic anomalies (a) are plotted separately from those showing none (b). HSE patterns for anomalous ureilites are repeated in (b) in the form of grey (DaG 319, Y 791538, EET 87517) and orange (ALHA 81101, A 881931) bands for visual comparison. Dashed lines represent literature data for the same ureilite (Rankenburg et al., 2008). (For interpretation of the references to color in this figure legend, the reader is referred to the web version of this article.)

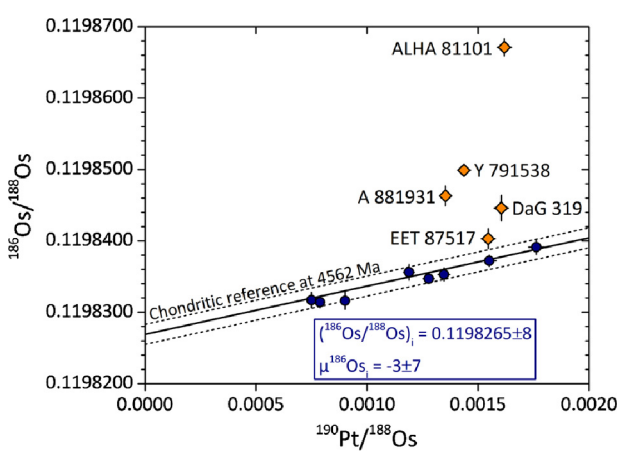

Fig. 2. Pt–Os isotopic data for ureilites. Five ureilite samples (orange diamonds) plot above the chondritic reference uncertainty envelope, showing nucleosynthetic anomalies in ^{186}Os dominating over the radiogenic contribution from ^{190}Pt decay (ureilite age of ∼4562 Ma based on ^{53}Mn–^{53}Cr and ^{26}Al–^{26}Mg; Goodrich et al., 2002; Kita et al., 2003). Eight other ureilite samples that show no nucleosynthetic anomalies (blue circles) plot within a band defined by the ingrowth of radiogenic ^{186}Os in chondrites (Brandon et al., 2005), and share the Solar System initial $^{186}Os/^{188}Os$ of 0.1198265 ± 8 and 0.1198269 ± 14, respectively. Note that the total radiogenic ingrowth of $\mu^{186}Os$ in a chondritic system is ∼110 ppm, compared with the larger effects observed due to nucleosynthetic contributions. (For interpretation of the references to color in this figure legend, the reader is referred to the web version of this article.)

run on the Faraday cups at signal intensities of approximately 3 V on $^{192}Os^{16}O_3^-$.

The spiked aliquots were processed using the same Os separation and purification procedure as the unspiked sample aliquots. Osmium concentrations were determined using the electron multiplier of the ThermoFisher Triton Plus at the University of Houston collecting 150 cycles with 16 s integration time in static mode. After Os extraction, the aqua regia fraction containing all other HSEs was dried down, converted to chloride form by repeated redissolution in 6 M HCl, and the HSEs were group-separated using the Eichrom™ AG50W-X8 100–200 mesh cation resin following the procedure of Puchtel and Humayun (2001, 2005). When required, the cation exchange HSE separation was repeated. The cuts containing the HSEs were dried down and re-dissolved in dilute HNO_3 and analyzed for HSE contents using a Thermo Electron Element 2 at Florida State University. Total analytical blanks ($N = 8$) averaged 12 ± 10 pg Ru, 21 ± 28 pg Pd, 1.1 ± 1.8 pg Re, 4.3 ± 5.8 pg Os, 4.3 ± 4.3 pg Ir, and 25 ± 25 pg Pt (2σ). Corrections to calculated concentrations from blank contributions were smaller than 1% for Re, Ru, Ir, Os, and Pt. Corrections on Pd concentrations were smaller than 4%. Based on the internal precision of individual ID-ICP-MS runs for the determination of HSE concentrations, the uncertainties used in calculations were 2.8% for Re, 0.2% for Os, 2% for Ir and Ru, 1.8% for Pt, and 3% for Pd ($2\sigma_{mean}$). These uncertainties do not include systematic weighing errors associated with the aliquoting that increase the uncertainties on the abundances. In this way, the reported uncertainties reflect only the precision of element ratios.

3. Results

The high-precision Os isotope data obtained for 12 monomict ureilites and polymict DaG 319 are reported in Table 1 and Supplementary Table 1. The highly siderophile element concentrations, Re/Os, Pt/Os, and $^{190}Pt/^{188}Os$, together with mineral assemblage, shock level, and Re abundances calculated from $^{187}Os/^{188}Os$ isotope ratios and measured Os abundances (Rankenburg et al., 2007), are presented in Table 2. For some ureilites (e.g., A 881931, Y 981750, and Y 981810), these are the first available HSE abundances. The HSE abundances obtained in this study are in reasonable agreement with prior published data for the same samples (Rankenburg et al., 2007, 2008) as shown in Fig. 1. Patterns of HSE concentration normalized to CI chondrites (Walker et al., 2002; Horan et al., 2003; Fischer-Gödde et al., 2010; Table 2) are relatively flat, ranging from ∼0.1 times CI in ALHA 81101 to ∼2.2 times CI in Y 981810 (Fig. 1), slightly lower than the ∼2.5 times CI reported for ALHA 78019 by Rankenburg et al. (2008). Calculated Re abundances based on the measured Os isotope ratios and abundances follow the same unfractionated, flat pattern of the refractory HSE (Fig. 1). However, all characterized ureilites, with the exception of ALHA 81101 and A 881931, show considerable depletion in Pd, a feature expected of restitic metal. The CI chondrite-normalized Pd/Os ratios of ureilites analyzed here (excluding ALHA 81101, A 881931, and sample duplicates) average 0.21 ± 0.25 (2σ), indistinguishable from the value of 0.19 ± 0.23 (2σ) reported by Rankenburg et al. (2008), but distinct from ALHA 81101 and A 881931 $(Pd/Os)_{CI}$ ranging between 0.71 and 0.95. The CI-normalized Pt/Os ratios for ureilites reported here average to 0.70 ± 0.38 (2σ), similar to the ratio of 0.74 ± 0.27 (2σ) calculated by Rankenburg et al. (2008), and the $(Pt/Os)_{CI}$ ratios of 0.71 to 0.88 measured for ALHA 81101 and A 881931.

The ureilite $^{187}Os/^{188}Os$ ratios determined in this work vary between 0.11663 and 0.12814 with a mean of 0.1256 ± 0.0060 (2σ) (Supplementary Table 1), comparable to the range of 0.11739 to 0.13018 and mean of 0.1259 ± 0.0046 (2σ) measured by Rankenburg et al. (2007) and interpreted to reflect a deriva-

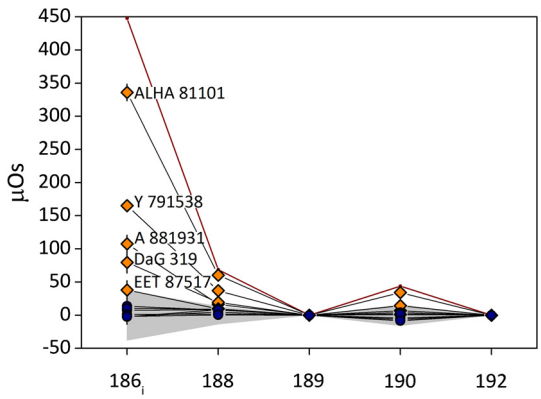

Fig. 3. Normalized high-precision Os isotopic compositions for ureilites. Error bars represent the $2\sigma_{mean}$ on the individual measurements including propagation of the Pt/Os uncertainties for $\mu^{186}Os_i$ ($\mu^{186}Os$ corrected to initial at T = 4.562 Ga), grey shaded area represents 2σ on UMD Os standard measurements (Supplementary Table 1). Samples with resolved Os isotope anomalies are labeled using orange diamonds. Red line indicates expected nucleosynthetic anomalies in Os due to an s-process excess of 0.05% using s-process yields from Arlandini et al. (1999). (For interpretation of the references to color in this figure legend, the reader is referred to the web version of this article.)

tion of ureilites from carbonaceous chondrite-like material. On a Re–Os isochron diagram (Supplementary Fig. 2), most data lie on a zero-age isochron indicating recent Re mobilization, with weathered samples showing the widest spread in $^{187}Re/^{188}Os$ (e.g., EET 87517 with minor to severe rustiness; Rankenburg et al., 2007). For 8 of the 13 ureilites analyzed, the $^{186}Os/^{188}Os$ ratio correlates well with Pt/Os ratios, plotting along the chondritic reference line, while 5 ureilites plot above the chondritic reference line (Fig. 2). Using measured $^{190}Pt/^{188}Os$ ratios (Table 2), the calculated initial $^{186}Os/^{188}Os$ ratios vary between 0.1198255 ± 13 and 0.1198561 ± 14 (Supplementary Table 1) including propagation of the Pt/Os ratio uncertainties, comparable to and significantly higher than a Solar System initial $^{186}Os/^{188}Os$ of 0.1198269 ± 14, determined using equilibrated H-type ordinary chondrites (Brandon et al., 2005). As outlined above, the high-precision Os isotopic data are also normalized to $^{192}Os/^{189}Os$, where both isotopes have only minor s-process contribution, to study nucleosynthetic isotope variation. To compare these data to earlier work, the μ notation is used for ^{186}Os, ^{188}Os, and ^{190}Os, as ppm deviation from the average chondritic reference value, and ε notation, as deviation in parts per 10,000 for ^{184}Os (Table 1; Supplementary Table 1).

4. Discussion

The isotope ^{186}Os is s-process-dominated, with a 1.1% p-process contribution (Arlandini et al., 1999). The ^{187}Os isotope is also an s-process-dominated isotope, but radiogenic decay from ^{187}Re overwhelms any identifiable nucleosynthetic isotope anomalies. The high-precision Os isotopic compositions for 8 ureilites, normalized to the r-process dominated $^{189}Os/^{192}Os$ ratio and average Solar System composition, fall within the $\pm 2\sigma$ uncertainty envelope of the terrestrial UMD standard determined by repeated analysis (external precision; Fig. 3). To obtain $\mu^{186}Os_i$, the $^{186}Os/^{189}Os$ ratios are corrected to their initial values at 4.562 Ga using the determined Pt/Os ratios (Table 2) and normalized to the time-equivalent ratios calculated for equilibrated H-type ordinary chondrites (Brandon et al., 2005). The preferred age of ~4562 Ma is based on the ^{53}Mn–^{53}Cr and ^{26}Al–^{26}Mg isotope systematics of ureilites (Goodrich et al., 2002; Kita et al., 2003). Five other ureilites (A 881931, ALHA 81101, DaG 319, EET 87517, and Y 791538) plot above this uncertainty envelope, most prominently for $\mu^{186}Os_i$. These 5 divergent ureilites exhibit correlated isotope anomalies

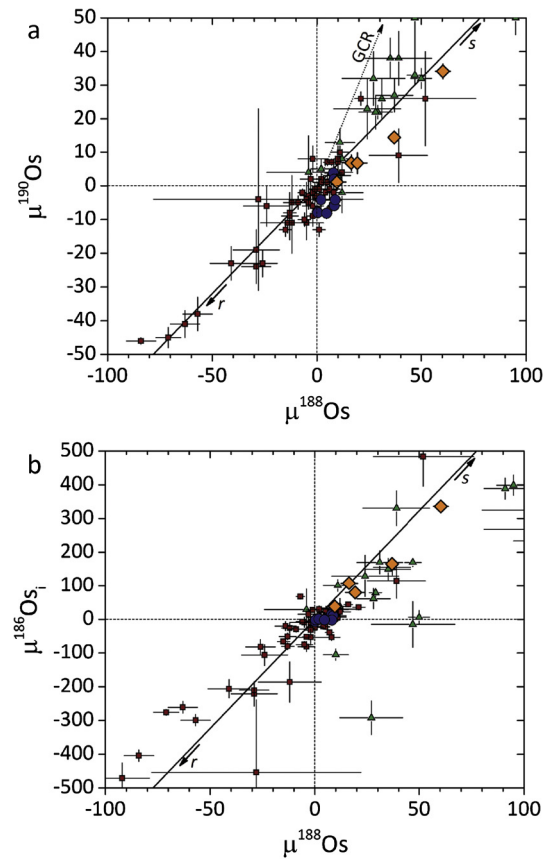

Fig. 4. $\mu^{190}Os$ (a) and $\mu^{186}Os_i$ (b) versus $\mu^{188}Os$ for bulk chondrite leachates (brown rectangles; Brandon et al., 2005; Reisberg et al., 2009; van Acken et al., 2011; Yokoyama et al., 2007, 2010), chondrite acid residues (green triangles; Yokoyama et al., 2007, 2010; 2011), and ureilites (orange diamonds and blue circles; this study). Terrestrial values are at zero. The $\pm 2\sigma_{mean}$ error bars on individual measurements are shown (internal precision). Five ureilites (in orange) show resolved isotope anomalies in $\mu^{190}Os$, $\mu^{188}Os$ and $\mu^{186}Os_i$. A trend for secondary neutron capture effects due to galactic cosmic ray (GCR) irradiation on the Os isotopic compositions of IVB magmatic iron meteorites (Wittig et al., 2013), different from the observed slope for ureilites, is depicted by the dotted arrow in (a). The five isotopically anomalous ureilites plot along a mixing line between solar and s-process Os components from the "stellar model" of Arlandini et al. (1999). (For interpretation of the references to color in this figure legend, the reader is referred to the web version of this article.)

of up to $\mu^{188}Os = 60 \pm 4$ ppm and $\mu^{190}Os = 34 \pm 2$ ppm in ALHA 81101 (Fig. 4). Similarly, the nucleosynthetic anomalies in ^{186}Os dominate over the radiogenic contribution from ^{190}Pt decay for these 5 ureilites (Fig. 2). Correcting for radiogenic ingrowth results in the largest observed anomaly of $\mu^{186}Os_i = 336 \pm 13$ ppm in ALHA 81101, followed by $\mu^{186}Os_i = 165 \pm 9$ ppm in Y 791538, $\mu^{186}Os_i = 108 \pm 13$ ppm in A 881931, $\mu^{186}Os_i = 80 \pm 16$ ppm in DaG 319, and $\mu^{186}Os_i = 38 \pm 14$ ppm in EET 87517, all correlating with their corresponding $\mu^{188}Os$ (Fig. 4b). The $\mu^{186}Os_i$, $\mu^{188}Os$, and $\mu^{190}Os$ measured for these 5 ureilites follow a mixing trend between average solar system Os (μOs = 0) and s-process Os (Arlandini et al., 1999; Fig. 4). As nearly 60% of all ureilites have cosmic-ray exposure ages less than 10 Ma (including ALHA 81101; Rai et al., 2003b) and an exposure age of 100 Ma is required for a shift of 0.2–1 epsilon units (Brandon et al., 2005), effects from cosmic-ray exposure are negligible. This is confirmed by the trend for secondary neutron-capture effects on Os from galactic cosmic ray (GCR) irradiation observed in iron meteorites (Walker, 2012; Wittig et al., 2013), which has a distinct and steeper slope from that for ureilites and chondrite leachates and residues for $\mu^{188}Os$ versus $\mu^{190}Os$ (Fig. 4a). The Os isotope anomalies of ALHA 81101 are roughly equal in magnitude but opposite in sign to

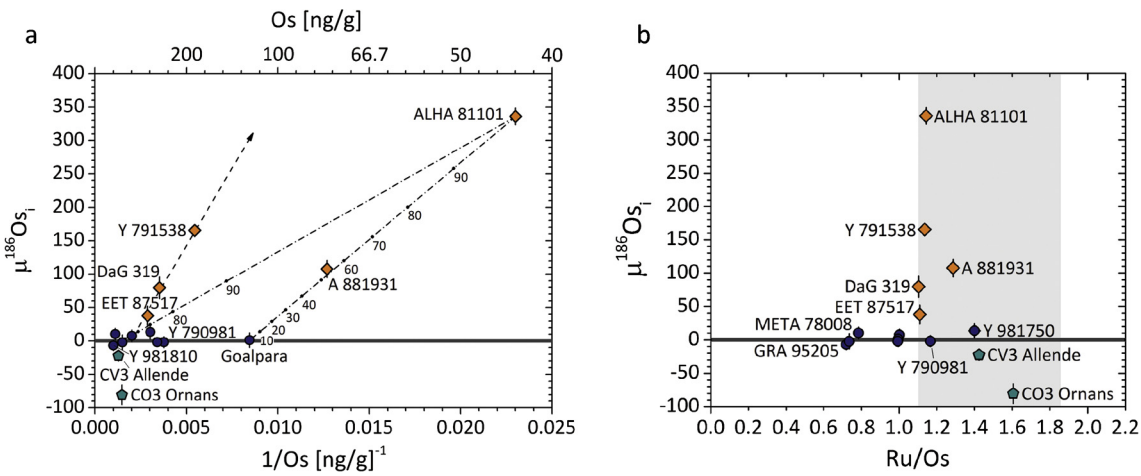

Fig. 5. (a) Plot of age-corrected $\mu^{186}Os_i$ versus inverse Os concentrations, showing admixtures of 10–90 vol% of ALHA 81101 to Goalpara and Y 981810 (dash-dotted lines). As evidenced by the Os isotope compositions of various ureilites with moderate s-process excesses (polymict DaG 319, and monomict EET 87517 and Y 791538), mixing is not restricted to two unique components. The Os isotopic compositions of these three ureilites require the existence of yet unsampled components (indicated by the dashed arrow) with higher Os content but Os isotopic signature similar to ALHA 81101 or even larger nucleosynthetic anomalies (i.e., $\mu^{186}Os_i > +1000$) for Os concentrations comparable to ALHA 81101. Such ureilite compositions likely represent zones in the UPB where metallic melt extraction was highly efficient. (b) Plot of $\mu^{186}Os_i$ versus Ru/Os, indicating that anomalous ureilites have Ru/Os ratios similar to chondrites (grey band).
Allende and Ornans chondrite data from Brandon et al. (2005).

the s-process Os isotope deficits reported for unequilibrated bulk chondrites using aqua regia digestion, interpreted to result from the presence of an insoluble s-process carrier (e.g., Brandon et al., 2005; van Acken et al., 2011). Solely based on Os isotopes, s-process enrichment/depletion can currently not be distinguished from r-process depletion/enrichment. Theoretically, based on the s-process yields of Arlandini et al. (1999), the distinction between s- and r-process could be made based on the ε^{184}Os data. However, the uncertainties associated with the ^{184}Os isotope ratio measurements are too large to resolve between r- or s-process contributions (cf. discussion in Brandon et al., 2005; Supplementary Table 1). Hence, anomalously high $\mu^{186}Os_i$ will be described as s-process excesses, while s-process deficits reflect anomalously low $\mu^{186}Os_i$, in accordance to previous work by Brandon et al. (2005), Reisberg et al. (2009), van Acken et al. (2011), and Yokoyama et al. (2007, 2010, 2011).

4.1. Osmium isotope anomaly carriers in the ureilite parent body

Osmium in chondrites may be hosted in Fe–Ni alloy, refractory metal nuggets, presolar SiC and graphite (e.g., Croat et al., 2005; Fischer-Gödde et al., 2010; Walker et al., 2002), but other presolar carriers are possible. As graphite is soluble in nitric acid and Os alloys are expected to dissolve in aqua regia, the likely carriers of the observed anomaly would have been consumed in the acid digestions, unless carried by an acid-resistant phase, such as SiC. Thermal metamorphism has been documented to destroy presolar graphite and SiC in chondrites with petrologic grades of more than 3.6 (Huss and Lewis, 1995). However, SiC grains survive better in the cases where reducing conditions prevailed during metamorphism, as observed by their presence in EH chondrites with metamorphic grades of >5 (Huss and Lewis, 1995). Although presolar grains have not been searched for in ureilites, presolar carriers might originally have been present in the carbonaceous vein material in ureilites. During partial melting, this carbonaceous material began to react with silicates, raising the Fo content of the olivine rims and reducing Fe to metal (Singletary and Grove, 2006). This reaction was quenched before completion as evidenced by the preservation of ferroan cores in olivines with residual interstitial carbonaceous phases in ureilites (e.g., Singletary and Grove, 2006). A plausible model for the precursors of ureilites would have a bulk solar Os isotopic composition, an s-process deficit in its metal, and a s-process excess in carbonaceous hosts of presolar origin. This model builds on the observation that the Os isotopic compositions of unequilibrated chondrites carrying presolar grains that have not been destroyed by thermal metamorphism, exhibit s-process deficits (Brandon et al., 2005; Reisberg et al., 2009; van Acken et al., 2011; Yokoyama et al., 2007, 2010, 2011). During partial melting, the isotopically distinct Os hosts evidently failed to equilibrate so that preferential extraction of s-process Os deficient metallic liquid created an enrichment in s-process Os in the residue. Thus, ureilites that have lost much of their Os during melt extraction exhibit large s-process excesses in their Os isotopes (Fig. 5).

4.2. Ureilite parent body reservoir mixing

Modeling in the Fe–S system by Rankenburg et al. (2008) indicates that HSE ratios in bulk ureilites could derive from carbonaceous chondrite-like precursors via extraction of 0 to >80% of their initial metal contents, with S-contents of the extracted metallic melts ranging from ∼15–30 wt% S. A positive shift in δ^{56}Fe compared to chondrites observed for ureilites, most pronounced for A 881931 and an ureilitic trachyandesitic clast (ALM-A) of the Almahata Sitta fall (ALHA 81101 was not measured), is in line with an efficient segregation of S-rich metallic melts at temperatures close to the Fe–FeS eutectic, before the onset of silicate melting (<1100 °C; Barrat et al., 2015). Metallic liquid (Fe–FeS) segregation can take place rapidly (timescale of <1 yr) when the matrix is deforming (Rushmer et al., 2005), while leaving residual Fe–Ni metal (Yoshino et al., 2004).

In this scenario, the subchondritic HSE abundances determined in most ureilites can be explained by mixing of distinct reservoirs in the UPB that were characterized by the formation of either partial or total metallic melts, depending on the local Fe_m/S ratio of the UPB zones. Ureilites characterized by superchondritic abundances of Re, Os, Ir, Ru, and Pt, but subchondritic Pd, and chondritic Os isotope compositions (e.g., Y 981810 and META 78008; Fig. 1b; Table 1; Supplementary Table 1), represent samples enriched in residual metal after extraction of a Fe–C–S metallic partial melt from carbonaceous chondrite-like precursor materials (Rankenburg et al., 2008; Hayden et al., 2011). The other ureilite composition, best represented by ALHA 81101 (Fig. 1a; Table 2), exhibits low HSE abundances in chondritic proportions,

but is enriched in s-process Os. These HSE-depleted ureilites with chondritic signatures (ALHA 81101 and A 881931) likely represent regions within the UPB, where metallic phases were completely molten and drained, while material with chondritic HSE abundances might have been added subsequently.

Osmium isotopic anomalies correlate inversely with the Os concentrations in ureilites, which can be produced by mixing between different UPB reservoirs (Fig. 5a). This mixing model requires more than two unique components. For example, Goalpara has an Os concentration lower than that of three other ureilites that exhibit Os isotope anomalies, but displays a chondritic Os isotopic composition. Curiously, Goalpara forms a mixing line with ALH 81101 that includes A 881931, both of the latter ureilites characterized by flat HSE patterns (Fig. 1a) and some of the largest anomalies reported (Figs. 2, 3, 4; Table 1; Supplementary Table 1). A mixing line between ALH 81101 and the majority of high-Os content ureilites does not form a good fit with the three remaining anomalous ureilites (Y 791538, DaG 319, and EET 87517), despite the observation that these share similar Pt/Os and Ru/Os ratios (Figs. 2 and 5b). Instead, mixing between the majority of ureilites analyzed here and an extrapolated component with higher Os concentrations or much larger isotopic anomaly in μOs than measured for ALHA 81101 is indicated by an arrow in Fig. 5a.

To estimate the possible timescales over which melt removal may have occurred, we estimated the Os diffusion length scale in metal or sulfide media. The diffusivity of Os has not been determined in metal, but can be assumed to be similar to that of Ir. At melt extraction temperatures in ureilites of ∼1150–1300 °C (Singletary and Grove, 2006), the diffusivity of Ir in Fe–Ni metal is $\sim 10^{-15}$ m^2/s (Righter et al., 2005). The diffusive homogenization time for a 100-μm metal grain is about 1 yr, and transport of Os across the hand specimen scale takes ∼1 Ma in solid metal. The diffusivity of Os in pyrrhotite at temperatures of ∼1300 °C is $\sim 10^{-12}$ m^2/s (Brenan et al., 2000), which would decrease the diffusive equilibration timescales to ∼3 h for a 100-μm grain and about 1000 yrs for hand specimen scale. Given the presence of large residual metallic grains in ureilites (∼10–40 μm in width; Goodrich et al., 2013), a brief heating event during an impact followed by burial (timescale ∼1 yr) would preserve Os isotopic heterogeneities more effectively than internal heating by ^{26}Al (timescale ∼1–2 Ma) that should eliminate such anomalies. Alternatively, physical modeling by Goodrich et al. (2007) implies that shallow melting (<30 bars) in the ureilite parent body may have resulted in melt extraction on timescales shorter than a year. The experimental studies of Yokoyama et al. (2009) highlight the difficulty of attaining Os isotopic equilibrium during melting, so that some form of disequilibrium melting is implied by the Os isotopic results in this study. Melt extraction in ureilites has been argued to be rapid and followed by intense disruption and brecciation of the UPB while hot (Goodrich et al., 2004, 2013). As such, ureilites sample mixtures of these UPB reservoirs combined in variable proportions (Fig. 5). Concurrent contamination of the reassembling materials with chondritic material derived from (an) impactor(s) may represent an additional component in the generation of present-day ureilite bulk rock siderophile element characteristics (Rankenburg et al., 2008; Fig. 5), although extracted metallic melts (e.g., Horstmann et al., 2014) might also be mixed back into ureilites with flat HSE patterns (Fig. 1).

4.3. Implications for other isotope systems

The rapid melting and mixing history of ureilites undoubtedly affected other presolar carriers, such as silicates and oxides, to differing extents resulting in hard to predict preservation of nucleosynthetic anomalies in other elements in ureilites that depends on the degree of isotopic equilibration attained. As such, the Os isotopic heterogeneity demonstrated here implies that isotopic anomalies reported for other elements, interpreted to reflect nebular heterogeneities (e.g., Andreasen and Sharma, 2007; Dauphas et al., 2002; Regelous et al., 2008; Trinquier et al., 2009), may partly or wholly result from parent body processing of carbonaceous chondritic precursors, a process that has not been considered before. Because ureilites are interpreted as restites (e.g., Goodrich et al., 2004; Singletary and Grove, 2006; Warren and Kallemeyn, 1992), the extracted metallic liquids and silicate liquids may have given rise to iron meteorites and achondritic basalts that bear reciprocal Os (and Cr, Ti, or Ni) isotopic anomalies. In this case, the isotopic anomalies produced in planetary differentiates do not reflect the isotopic composition of the bulk precursor body. Some workers consider ureilite melts to be removed by intense CO streaming leading to explosive volcanism (Warren and Kallemeyn, 1992), unlikely to form metallic or basaltic meteorites. In this case, the s-process deficit material was likely dispersed widely in the early Solar System, possibly accreting to new parent bodies. It should be noted that Os isotope ratios in bulk iron meteorites (Walker, 2012; Wittig et al., 2013) do not show resolvable isotope anomalies, while Mo, Ru and Pd from the same irons contain s-process deficits (e.g., Burkhardt et al., 2011; Chen et al., 2010; Mayer et al., 2015). The Mo and Ru isotopic compositions of ureilites are not known at present. However, the absence of a correlation between Mo and Os isotope anomalies for acid leachates and residues of the Murchison meteorite argues for a multitude of processes, including thermal nebular effects, and different presolar phases involved (e.g., Reisberg et al., 2009; Burkhardt et al., 2012). Oxygen and Os isotopes both indicate that ureilites originated from carbonaceous chondrite-like precursors (Clayton and Mayeda, 1996; Rankenburg et al., 2007). Until the issue of differential melting has been taken into account, endemic isotope anomalies in Ti, Cr and Ni cannot be used to refute genetic links between ureilites and potential carbonaceous chondritic precursors (Warren, 2011).

4.4. Implications for the isotopic composition of the Earth

There are two sets of nucleosynthetic anomalies that constrain the formation of Earth, Moon, and Mars as well as the other terrestrial planets from chondritic or achondritic precursors. Isotope anomalies in the elements of or adjacent to the Fe-peak (including Ti, Cr, and Ni) indicate that carbonaceous chondrites constituted a minor mass fraction of the inner planets, while E- and O-chondrites are isotopically similar to these planets (e.g., Regelous et al., 2008; Trinquier et al., 2009; Warren, 2011). Based on Fe-peak anomalies, the Earth, Moon and Mars could be sourced from a variety of achondritic and chondritic planetesimals. This is not the case for isotope anomalies in elements beyond the Fe-peak, where all known chondritic and differentiated bodies exhibit s-process deficits in Mo and Ru isotope anomalies relative to the Earth (e.g., Burkhardt et al., 2011; Chen et al., 2010). The fact that the Earth exhibits higher proportions of s-process nuclides than all analyzed chondritic and differentiated bodies in Mo (Burkhardt et al., 2011; Dauphas et al., 2002), Ru (Chen et al., 2010), and Nd (Boyet and Carlson, 2005) isotopes requires that a major portion of the terrestrial mix of planetesimals marked by s-process excesses has not been sampled, yet. The ureilites are the first candidates for this missing component. The presence of s-process excesses in Os isotopic compositions for ureilites could indicate that the Earth preferentially accreted olivine-rich restites, consistent with its high Mg/Si non-chondritic composition (Caro and Bourdon, 2010). As aubrites, the achondritic counterparts to enstatite chondrites, do not show Os isotope anomalies (van Acken et al., 2011), continued efforts to characterize differentiated planetary materials for a range of elements affected by nucleosynthetic

isotope effects may confirm if the circumstances leading to isotopically distinct planetary reservoirs were unique to the UPB.

5. Conclusions

In this study, we report the first s-process excesses in Os isotopes in bulk ureilites. In contrast to previously reported isotope anomalies in achondrites, the new results show a range of isotope anomalies among ureilites, from non-anomalous ureilites to variable degrees of s-process isotope excess anti-correlated with Os abundances in 5 ureilites. These results stand in stark contrast to the isotopic homogeneity of Os among all bulk Solar System materials characterized to date, and to the isotopic variability recorded in siderophile Mo, Ru, Pd, and W for differentiated meteorites (e.g., Burkhardt et al., 2011; Chen et al., 2010; Dauphas et al., 2002; Mayer et al., 2015; Qin et al., 2008). Further, in contrast to the aforementioned Mo, Ru and Pd isotope anomalies which all exhibit s-process isotope deficits, ureilites exhibit the first s-process excesses (relative to terrestrial isotope abundances) in an element (Os) for which bulk chondrites exhibit no anomalies. Thus, it is clear that the reported Os anomalies were expressed by the planetary differentiation of ureilites that resulted in losses of s-deficit Os in metallic liquids. This s-deficit material may have been lost from the ureilite parent body by explosive volcanism, and may have been accreted by other bodies in the early Solar System. The assumption that melting would homogenize any existing isotope anomalies had already been disproved for oxygen isotopes in primitive achondrites (Clayton and Mayeda, 1996). Here, we extend that result to Os isotopes. To preserve these Os isotopic heterogeneities, rapid melting of ureilites is essential. The melting timescale of ureilites has been constrained here to around a year or less, consistent with an impact heat source for ureilite melting, or with disequilibrium melting during explosive volcanism for ureilites.

As presolar phases release their nucleosynthetic components at variable rates during the melting of a meteorite parent body, therefore, the isotopic compositions for a range of elements (e.g., Ti, Cr, Ni, Mo, Ru, Os) might not be primary characteristics of precursor materials, limiting their use as provenance indicators. This is demonstrated compellingly here for ureilites, previously argued to derive from non-carbonaceous chondritic precursors based on Ti, Cr, and Ni isotopic compositions (Warren, 2011) despite oxygen (Clayton and Mayeda, 1996) and osmium (Rankenburg et al., 2007) isotope evidence for a carbonaceous chondritic parent. The presence of s-process excesses in Os isotopic compositions for ureilites could also indicate that if the Earth preferentially accreted olivine-rich restites, then it could have inherited a s-process excess relative to smaller meteorite bodies, consistent with its high Mg/Si composition, and the fact that Earth exhibits an enrichment of s-process nuclides in Mo, Ru, and Nd isotopes. Further studies of heavy element isotope anomalies in ureilites are required to establish whether such isotope anomalies can be used as indicators of provenance or of process.

Acknowledgements

We thank the Smithsonian Institution, NASA and the Japanese National Institute of Polar Research for samples. This work was funded by NASA grants to ADB (NNX12AD06G) and MH (NNX13AI06G). SG is a Postdoctoral Fellow of the Research Foundation Flanders (FWO). Additional support to SG was provided by the Interuniversity Attraction Poles Program Planet Topers initiated by the Belgian Science Policy Office, Vocatio and the Ernest Solvay Fund managed by the King Baudouin Foundation, and the VUB Strategic Research Council. Constructive and meticulous reviews by T. Kleine, L. Reisberg, and editor B. Marty are gratefully acknowledged.

Appendix A. Supplementary material

Supplementary material related to this article can be found online at http://dx.doi.org/10.1016/j.epsl.2015.09.021.

References

Akram, W., Schönbächler, M., Bisterzo, S., Gallino, R., 2015. Zirconium isotope evidence for the heterogeneous distribution of s-process materials in the solar system. Geochim. Cosmochim. Acta 165. http://dx.doi.org/10.1016/j.gca.2015.02.013.

Andreasen, R., Sharma, M., 2007. Mixing and homogenization in the early solar system: clues from Sr, Ba, Nd, and Sm isotopes in meteorites. Astrophys. J. 665, 874–883.

Arlandini, C., Käppeler, F., Wisshak, K., Gallino, R., Lugaro, M., Busso, M., Straniero, O., 1999. Neutron capture in low-mass asymptotic giant branch stars: cross sections and abundance signatures. Astrophys. J. 525, 886–900.

Barrat, J.A., Rouxel, O., Wang, K., Moynier, F., Yamaguchi, A., Bischoff, A., Langlade, J., 2015. Early stages of core segregation recorded by Fe isotopes in an asteroidal mantle. Earth Planet. Sci. Lett. 419, 93–100.

Begemann, F., Ludwig, K.R., Lugmair, G.W., Min, K., Nyquist, L.E., Patchett, P.J., Renne, P.R., Shih, C.-Y., Villa, I.M., Walker, R.J., 2001. Call for an improved set of decay constants for geochronological use. Geochim. Cosmochim. Acta 65, 111–121.

Birck, J.L., Barman, M.R., Capmas, F., 1997. Re–Os isotopic measurements at the femtomole level in natural samples. Geostand. Newsl. – J. Geostand. Geoanal. 21, 19–27.

Boyet, M., Carlson, R.W., 2005. ^{142}Nd evidence for early (>4.53 Ga) global differentiation of the silicate Earth. Science 309, 576–581.

Brandon, A., Humayun, M., Puchtel, I.S., Leya, I., Zolensky, M., 2005. Osmium isotope evidence for an s-process carrier in primitive chondrites. Science 309, 1233–1236.

Brenan, J.M., Cherniak, D.J., Rose, L.A., 2000. Diffusion of osmium in pyrrhotite and pyrite: implications for closure of the Re–Os isotopic system. Earth Planet. Sci. Lett. 180, 399–413.

Burkhardt, C., Kleine, T., Oberli, F., Pack, A., Bourdon, B., Wieler, R., 2011. Molybdenum isotope anomalies in meteorites: constraints on solar nebula evolution and origin of the Earth. Earth Planet. Sci. Lett. 312, 390–400.

Burkhardt, C., Kleine, T., Dauphas, N., Wieler, R., 2012. Origin of isotopic heterogeneity in the solar nebula by thermal processing and mixing of nebular dust. Earth Planet. Sci. Lett. 357, 298–307.

Carlson, R.W., Boyet, M., Horan, M., 2007. Chondrite barium, neodymium, and samarium isotopic heterogeneity and early earth differentiation. Science 316, 1175–1178.

Caro, G., Bourdon, B., 2010. Non-chondritic Sm/Nd ratio in the terrestrial planets: consequences for the geochemical evolution of the mantle-crust. Geochim. Cosmochim. Acta 74, 3333–3349.

Chen, J.H., Papanastassiou, D.A., Wasserburg, G.J., 2010. Ruthenium endemic isotope effects in chondrites and differentiated meteorites. Geochim. Cosmochim. Acta 74, 3851–3862.

Clayton, R.N., Mayeda, T.K., 1996. Oxygen isotope studies of achondrites. Geochim. Cosmochim. Acta 60, 1999–2017.

Cohen, A.S., Waters, F.J., 1996. Separation of osmium from geological materials by solvent extraction for analysis by thermal ionisation mass spectrometry. Anal. Chim. Acta 332, 269–275.

Croat, T.K., Stadermann, F.J., Bernatowicz, T.J., 2005. Presolar graphite from AGB stars: microstructure and s-process enrichment. Astrophys. J. 631, 976–987.

Dauphas, N., Marty, B., Reisberg, L., 2002. Molybdenum nucleosynthetic dichotomy revealed in primitive meteorites. Astrophys. J. 569, L139–L142.

Farquhar, J., Jackson, T.L., Thiemens, M.H., 2000. A ^{33}S enrichment in ureilite meteorites: evidence for a nebular sulfur component. Geochim. Cosmochim. Acta 64, 1819–1825.

Fischer-Gödde, M., Becker, H., Wombacher, F., 2010. Rhodium, gold and other highly siderophile element abundances in chondritic meteorites. Geochim. Cosmochim. Acta 74, 356–379.

Goodrich, C.A., Hutcheon, I.D., Keil, K., 2002. ^{53}Mn–^{53}Cr age of a highly-evolved, igneous lithology in polymict ureilite DaG 165. In: 65th Annual Meeting of the Meteoritical Society. 5190 (Abst.).

Goodrich, C.A., Scott, E.R.D., Fioretti, A.M., 2004. Ureilitic breccias: clues to the petrologic structure and impact disruption of the ureilite parent asteroid. Chem. Erde – Geochem. 64, 283–327.

Goodrich, C.A., Van Orman, J.A., Wilson, L., 2007. Fractional melting and smelting on the ureilite parent body. Geochim. Cosmochim. Acta 71, 2876–2895.

Goodrich, C.A., Ash, R.D., Van Orman, J.A., Domanik, K., McDonough, W.F., 2013. Metallic phases and siderophile elements in main group ureilites: implications for ureilite petrogenesis. Geochim. Cosmochim. Acta 112, 340–373.

Hayden, L.A., Van Orman, J.A., McDonough, W.F., Ash, R.D., Goodrich, C.A., 2011. Trace element partitioning in the Fe–S–C system and its implications for planetary differentiation and the thermal history of ureilites. Geochim. Cosmochim. Acta 75, 6570–6583.

Horan, M.F., Walker, R.J., Morgan, J.W., Grossman, J.N., Rubin, A.E., 2003. Highly siderophile elements in chondrites. Chem. Geol. 196, 5–20.
Horstmann, M., Humayun, M., Fischer-Gödde, M., Bischoff, A., Weyrauch, M., 2014. Si-bearing metal and niningerite in Almahata Sitta fine-grained ureilites and insights into the diversity of metal on the ureilite parent body. Meteorit. Planet. Sci. 49, 1948–1977.
Huss, G.R., Lewis, R.S., 1995. Presolar diamond, SiC, and graphite in primitive chondrites: abundances as a function of meteorite class and petrologic type. Geochim. Cosmochim. Acta 59, 115–160.
Kita, N.T., Ikeda, Y., Togashi, S., Shimoda, G., Morishita, Y., Weisberg, M.K., 2003. Evolution of ureilites by Al-26 heating of the parent body. Geochim. Cosmochim. Acta 67 (18), A220 (Abst.).
Mayer, B., Wittig, N., Humayun, M., Leya, I., 2015. Palladium isotopic evidence for nucleosynthetic and cosmogenic isotope anomalies in IVB iron meteorites. Astrophys. J. 809, 180. http://dx.doi.org/10.1088/0004-637X/809/2/180.
Puchtel, I.S., Humayun, M., 2001. Platinum group element fractionation in a komatiitic basalt lava lake. Geochim. Cosmochim. Acta 65, 2979–2993.
Puchtel, I.S., Humayun, M., 2005. Highly siderophile element geochemistry of ^{187}Os-enriched 2.8 Ga Kostomuksha komatiites, Baltic Shield. Geochim. Cosmochim. Acta 69, 1607–1618.
Qin, L., Dauphas, N., Wadhwa, M., Markowski, A., Gallino, R., Janney, P.E., Bouman, C., 2008. Tungsten nuclear anomalies in planetesimal cores. Astrophys. J. 674, 1234–1241.
Qin, L., Alexander, C.M.O'D., Carlson, R.W., Horan, M.F., Yokoyama, T., 2010. Contributors to chromium isotope variation of meteorites. Geochim. Cosmochim. Acta 74, 1122–1145.
Rai, V.K., Murty, S.V.S., Ott, U., 2003a. Nitrogen components in ureilites. Geochim. Cosmochim. Acta 67, 2213–2237.
Rai, V.K., Murty, S.V.S., Ott, U., 2003b. Noble gases in ureilites: cosmogenic, radiogenic, and trapped components. Geochim. Cosmochim. Acta 67, 4435–4456.
Rankenburg, K., Brandon, A.D., Humayun, M., 2007. Osmium isotope systematics of ureilites. Geochim. Cosmochim. Acta 71, 2402–2413.
Rankenburg, K., Humayun, M., Brandon, A.D., Herrin, J.S., 2008. Highly siderophile elements in ureilites. Geochim. Cosmochim. Acta 72, 4642–4659.
Regelous, M., Elliott, T., Coath, C.D., 2008. Nickel isotope heterogeneity in the early solar system. Earth Planet. Sci. Lett. 272, 330–338.
Reisberg, L., Dauphas, N., Luguet, A., Pearson, D.G., Gallino, R., Zimmermann, C., 2009. Nucleosynthetic osmium isotope anomalies in acid leachates of the Murchison meteorite. Earth Planet. Sci. Lett. 277, 334–344.
Righter, K., Campbell, A.J., Humayun, M., 2005. Diffusion of trace elements in FeNi metal: application to zoned metal grains in chondrites. Geochim. Cosmochim. Acta 69, 3145–3158.
Rushmer, T., Petford, N., Humayun, M., Campbell, A.J., 2005. Fe-liquid segregation in deforming planetesimals: coupling core-forming compositions with transport phenomena. Earth Planet. Sci. Lett. 239, 185–202.
Singletary, S., Grove, T.L., 2006. Experimental constraints on ureilite petrogenesis. Geochim. Cosmochim. Acta 70, 1291–1308.
Smoliar, M.I., Walker, R.J., Morgan, J.W., 1996. Re–Os ages of group IIA, IIIA, IVA, and IVB iron meteorites. Science 271, 1099–1102.
Sprung, P., Scherer, E.E., Upadhyay, D., Leya, I., Mezger, K., 2010. Non-nucleosynthetic heterogeneity in non-radiogenic stable Hf isotopes: implications for early solar system chronology. Earth Planet. Sci. Lett. 295, 1–11.
Trinquier, A., Elliott, T., Ulfbeck, D., Coath, C., Krot, A.N., Bizzarro, M., 2009. Origin of nucleosynthetic isotope heterogeneity in the solar protoplanetary disk. Science 324, 374–376.
van Acken, D., Brandon, A.D., Humayun, M., 2011. High precision osmium isotopes in enstatite and Rumuruti chondrites. Geochim. Cosmochim. Acta 75, 4020–4036.
Walker, R.J., 2012. Evidence for homogeneous distribution of osmium in the protosolar nebular. Earth Planet. Sci. Lett. 351–352, 36–44.
Walker, R.J., Horan, M.F., Morgan, J.W., Becker, H., Grossman, J.N., Rubin, A.E., 2002. Comparative ^{187}Re–^{187}Os systematics of chondrites: implications regarding early solar system processes. Geochim. Cosmochim. Acta 66, 4187–4201.
Warren, P.H., 2011. Stable isotopes and the noncarbonaceous derivation of ureilites in common with nearly all differentiated planetary materials. Geochim. Cosmochim. Acta 75, 6912–6926.
Warren, P.H., Kallemeyn, G.W., 1992. Explosive volcanism and the graphite–oxygen fugacity buffer on the parent asteroid(s) of the ureilite meteorites. Icarus 100, 110–126.
Warren, P.H., Ulff-Møller, F., Huber, H., Kallemeyn, G.W., 2006. Siderophile geochemistry of ureilites: a record of early stages of planetesimal core formation. Geochim. Cosmochim. Acta 70, 2104–2126.
Wittig, N., Humayun, M., Brandon, A.D., Huang, S., Leya, I., 2013. Couplet W–Os–Pt isotope systematics in IVB iron meteorites: in situ neutron dosimetry for W isotope chronology. Earth Planet. Sci. Lett. 361, 152–161.
Yin, Q., Jacobsen, S.B., Yamashita, K., 2002. Diverse supernova sources of presolar material inferred from molybdenum isotopes in meteorites. Nature 415, 881–883.
Yokoyama, T., Rai, V.K., Alexander, C.M.O'D., Lewis, R.S., Carlson, R.W., Shirey, S.B., Thiemens, M.H., Walker, R.J., 2007. Osmium isotope evidence for uniform distribution of s- and r-process components in the early solar system. Earth Planet. Sci. Lett. 259, 567–580.
Yokoyama, T., Walker, D., Walker, R.J., 2009. Low osmium solubility in silicate at high pressures and temperatures. Earth Planet. Sci. Lett. 279, 165–173.
Yokoyama, T., Alexander, C.M.O'D., Walker, R.J., 2010. Osmium isotope anomalies in chondrites: results for acid residues and related leachates. Earth Planet. Sci. Lett. 291, 48–59.
Yokoyama, T., Alexander, C.M.O'D., Walker, R.J., 2011. Assessment of nebular versus parent body processes on presolar components in chondrites: evidence from Os isotopes. Earth Planet. Sci. Lett. 305, 115–123.
Yoshino, T., Walter, M.J., Katsura, T., 2004. Connectivity of molten Fe alloy in peridotite based on in situ electrical conductivity measurements: implications for core formation in terrestrial planets. Earth Planet. Sci. Lett. 222, 625–643.
Zinner, E., 1998. Stellar nucleosynthesis and the isotopic composition of presolar grains from primitive meteorites. Annu. Rev. Earth Planet. Sci. 26, 147–188.